Experimental and Finite Element Analysis of an Electronic Pole-Change Drive

Mohamed Osama
General Electric Company
Corporate Research and Development Center
One Research Circle
Niskayuna, NY 12309

Thomas A. Lipo
University of Wisconsin - Madison
Department of Electrical and Computer Engineering
1415 Engineering Drive
Madison, WI 53706

***Abstract*- The theory and modeling of an electronic pole-change drive for the purpose of extending the constant power speed range of a four-pole induction machine, has been previously reported. This paper presents verification of the power capability characteristics of the proposed drive through experimental implementation. An indirect field oriented controller is developed for the pole-change drive with the estimated rotor open circuit time constant and d-axis current commands dependent on the mode of operation. It is demonstrated that for a constant power load, the drive can operate at 6340 rpm in two-pole mode without exceeding either the voltage or current limits at 3600 rpm in four-pole mode. A finite element method is also utilized to examine the influence of magnetic saturation on the pole-change drive performance. The nature of the magnetic flux distribution and saturation progression is investigated in both four-pole and two-pole modes. The saturation induced inductance variation is also studied and its influence on the *dq* inductance matrix is quantified.**

I. INTRODUCTION

High inertia traction loads (among other applications) require an electric drive capable of high torque at low speeds in addition to a constant output power wide speed range above rated speed. The traditional approaches to meet these requirements involved either oversizing of the machine and/or inverter, or modifying the machine magnetic structure design to decrease its leakage inductance [1]. Space constraints in certain drives make oversizing the machine nonfeasible while oversizing the inverter is uneconomical. Modifying the machine magnetic structure to decrease the leakage results in higher motor torque ripple and copper losses due to the increase in motor harmonic current components.

The induction machine equivalent per phase impedance (at a given speed) can be reduced by various stator winding change techniques including; Y-Δ changeover, winding tapping, series to parallel reconnection and reducing the pole number of a pole change winding. Recently, several of these methods have been re-introduced in adjustable speed drives for the purpose of extending the constant power speed range during field weakening for a field oriented drive [2-3]. This is achieved by operating at a large motor impedance till the maximum speed for constant power operation (about twice base speed). Switching to a lower motor impedance (using contactors) facilitates extending the constant power range without increasing the required motor voltage by re-adjusting the flux level. A previous paper [4] proposes a four/two-pole induction machine drive which achieves the desired torque-speed capability based on electronic pole-changing [5, 6]. In electronic pole-changing, the desired MMF distribution is attained by reversing the necessary coil groups currents instead of reversing their connections. Based on the same principle, an eight/four-pole induction motor drive is currently being developed for an electric vehicle application by Meidensha Corporation [7]. An electronic pole-changing drive avoids using any winding connection switching devices such as contactors. The total inverter rating is not increased while the motor is marginally oversized [8]. No change in the motor magnetic structure is required. On the other hand, the main limitations of such a drive are the need to access the individual machine coil groups, the additional control complexity and doubling of the number of inverter switches. This paper presents verification of the power capability characteristics of the four/two-pole drive through experimental implementation. An indirect field oriented controller is also developed based on a six dimensional reference frame model. In addition, the influence of magnetic saturation on the pole-change drive performance is investigated via finite element analysis.

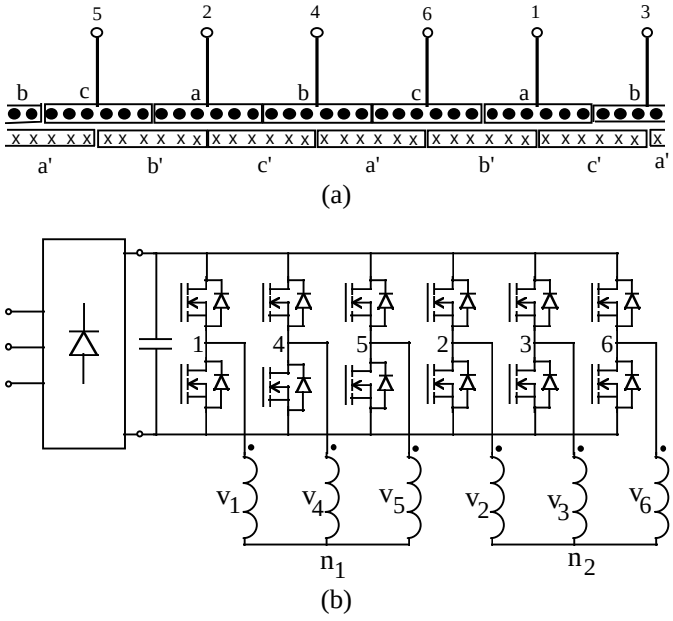

Fig. 1 Electronic pole-change drive used in experimental setup: (a) stator winding distribution (b) inverter topology

0-7803-5589-X/99/$10.00 (c) 1999

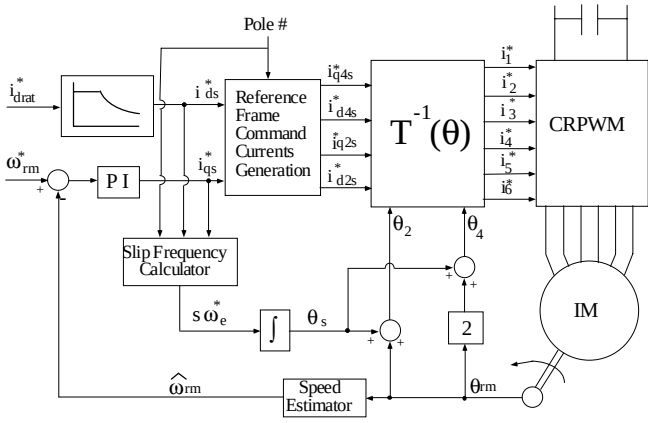

Fig. 2. Electronic pole-change drive with indirect field oriented control

II. Indirect Field Orientation Control For Pole-Change Drive

Figure 1a shows the four/two pole drive stator winding distribution which is a full pitch double layer 120^{o} phase belt. The two coil groups per phase are connected separately resulting in a six terminal stator (1-6). As illustrated by Fig. 1b, a six leg inverter is needed to supply this machine. The proposed drive operates as a four-pole machine from zero speed until the end of its constant power range (3600 rpm for 2 p.u overload torque capability). The constant power speed range is extended by employing "electronic" pole changing to obtain two-pole operation.

In order to compare the capability characteristics of the proposed drive in four-pole and two-pole operation, an indirect field orientation controller with an outside speed loop is implemented. As is illustrated in Fig. 2, several features distinguish this controller from those used in conventional three phase induction motor drives. The rotor open circuit time constant and d-axis current commands are both dependent on the mode of operation. A six dimensional transformation matrix (T(θ)) [8], is needed to transform between the coil group variables and the reference frame variables.

A. Relationship between d-axis currents and rotor flux

The principle of rotor flux orientation is to orient the d-axis of the synchronous reference frame to the rotor flux (resulting in $\lambda_{qr} = 0$ all the time). For a tuned system, instantaneous torque control is achieved via i_{qs} (if i_{ds} is kept constant), while $\boldsymbol{i_{ds}}$ determines the steady state rotor flux level [9];

$$T_e = \left(\frac{3}{2}\frac{P}{2}\frac{L_m}{L_r}\right)\lambda_{dr}\, i_{qs} \tag{1}$$

$$\lambda_r = \lambda_{dr} = \frac{L_m}{1+T_r s}\, i_{ds} \tag{2}$$

$$\lambda_r = \lambda_{dr} = \frac{L_m}{1+T_r s}\, i_{ds} \tag{3}$$

Thus the ratio between the d-axis current levels $(i_{d4s} \,\&\, i_{d2s})$ and rotor flux densities $(B_{r4} \,\&\, B_{r2})$ in four-pole and two-pole operation has to be known. In an induction machine, the magnetizing current is related to the air gap flux density by,

$$i_m = \frac{1}{L_m}\, k_w\, N_{ser}\, \frac{A_{tot}}{P}\, B_g \tag{4}$$

where

L_m	magnetizing inductance
k_w	winding factor
N_{ser}	total number of series turns per phase
A_{tot}	total air gap surface area
P	number of poles

Since $k_{w2} \approx 0.8 k_{w4}$ [4] for this stator winding ,

$$\frac{i_{m2}}{i_{m4}} = 1.6\,\frac{L_{m4}}{L_{m2}}\,\frac{B_{g2}}{B_{g4}} \tag{5}$$

For a field oriented machine, the ratio between the d-axis stator currents can be deduced from (3) and (5) as:

$$\frac{i_{d2s}}{i_{d4s}} = 1.6\,\frac{L_{m4}}{L_{m2}}\,\frac{(1+T_{r2}s)}{(1+T_{r4}s)}\,\frac{B_{r2}}{B_{r4}} \tag{6}$$

In steady state, (6) reduces to;

$$\frac{I_{d2s}}{I_{d4s}} = 1.6\,\frac{L_{m4}}{L_{m2}}\,\frac{B_{r2}}{B_{r4}} \tag{7}$$

As depicted in Fig. 2, above rated speed the d-axis current command $\left(i^{*}_{ds}\right)$ varies inversely with speed leading to the steady-state rotor flux density also varying inversely with speed (for tuned conditions). The q-axis current command $\left(i^{*}_{qs}\right)$ is determined by the output of a PI speed regulator that is tuned to a 5 Hz bandwidth. The mode of operation determines the slip frequency calculator estimate of the rotor time constant $\left(\hat{T}_{r4}\ or\ \hat{T}_{r2}\right)$ and also the d-axis current command level $\left(i^{*}_{d4s}\ or\ i^{*}_{d2s}\right)$ as decided by (7). The digital implementation of the slip frequency calculator can be expressed in the Z-domain as:

$$s\omega_e(z) = \frac{\dfrac{1}{\hat{T}_{rx}}\; i^{*}_{qs}(z)}{\left(1-e^{-\frac{T}{\hat{T}_{rx}}}\right)z^{-1}} \;\; \frac{}{1-z^{-1}e^{-\frac{T}{\hat{T}_{rx}}}}\; i^{*}_{dxs}(z) \tag{8}$$

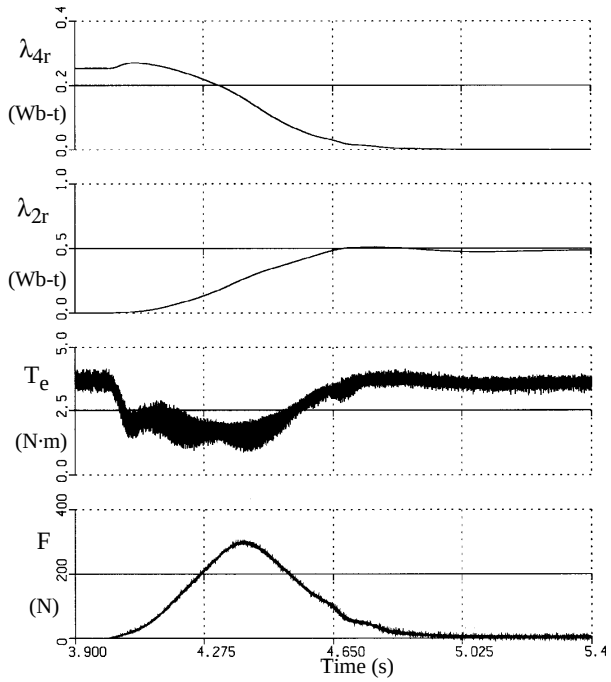

Fig. 3. Simulation results: Pole switching transition with indirect field oriented controller

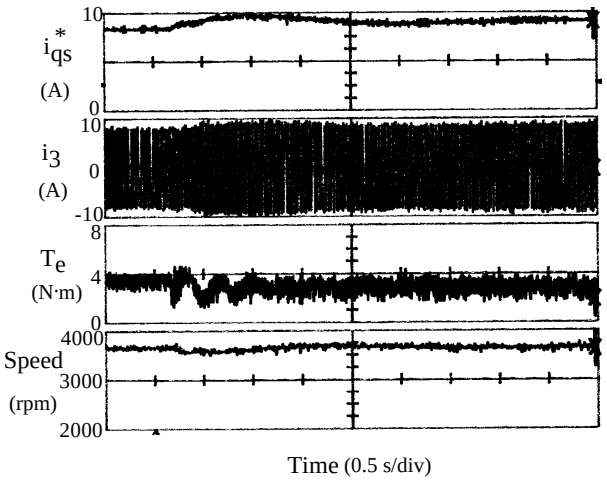

Fig. 4. Experimental results: Pole switching transition with indirect field oriented controller

x stands for 4 or 2 depending on mode of operation. The slip calculator tuning in both four-pole and two-pole operation is verified by ensuring a ramp speed response to a step change in i_{qs}^{*}.

B. *Pole Changing Transition*

The pole changing transition is implemented for the indirect field oriented control drive with a ramp change in the reference frame current commands in order to minimize the resulting torque transient. Since the overlap time (0.6 s) is longer than either T_{r4} or T_{r2}, the four-pole plane and two-pole plane rotor flux linkages have almost the same rise and decay rates as demonstrated by the simulation results of Fig. 3. Due to the pole changing occurring at one half rated flux (at a speed of 3650 rpm), the resultant radial force transient is one fourth that in case of slip frequency control drive [8]. The experimental results of Fig. 4 substantiate the reference frame model based simulation results.

III. Steady State Capability Curves

Two different loads are used to examine the performance of the proposed induction motor drive with indirect field orientation control. The first load is a hysteresis brake with a kinetic power rating of 1.3 kW making it a "limited" or constant power load. Due to a rotor peripheral speed limit of 7500 ft/min [10], the test motor has a mechanical speed limit of 6600 rpm.

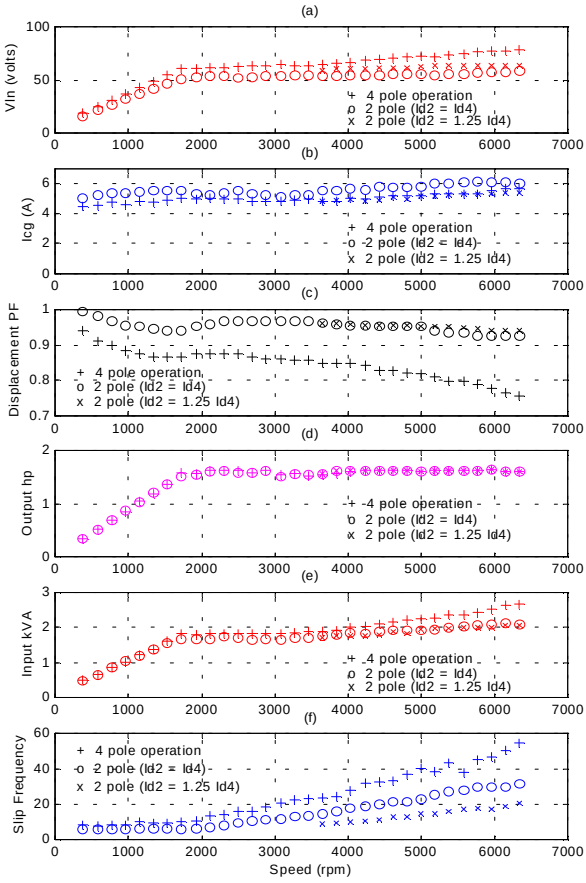

Fig. 5. Constant power load experimental results

A. *Constant Power Load*

Fig. 5 shows the steady state experimental test results for the proposed drive with the hysteresis brake load. The torque is almost constant (6.4 N·m) below 1730 rpm while

the output power is constant (1.6 hp) above 1730 rpm due to the load limitations.

From Fig. 5a, it is clear that the voltage of the power supply must continue to increase during the constant power region to counteract the increased voltage drop across the stator leakage inductance. For four-pole operation, the voltage increase at 3650 rpm is 6.6% of the rated voltage (at 1730 rpm) while the rate of voltage increase is higher above this speed to reach 29% of rated voltage at 6340 rpm. During field weakening the average magnetizing inductance ratio is $\frac{L_{m2}}{L_{m4}} = 1.6$, thus if the d-axis current for two-pole operation is kept the same as four-pole operation, the rotor flux density would be the same in both modes (from (7)). This would mean approximately the same air gap flux density and hence the two-pole air gap voltage would be about 80% that of four-pole. Although the power factor for two-pole operation is higher than four-pole (Fig. 5c), a 10%-15% increase in input current is required for the same output power. From Fig. 5e, the input kVA is lower for two-pole while the slip frequency is about 60% of that of four-pole (Fig. 5f). The motor has higher efficiency in four-pole operation below a speed of about 3500 rpm while at higher speeds, the losses (and hence efficiency) are approximately the same in both operation modes.

The maximum output torque and current developed by the machine is ultimately dependent on the allowable inverter current rating and the maximum voltage which the inverter can apply to the machine. Thus for two-pole operation above 3600 rpm, increasing I^*_{ds2} by 25% would result in the same back EMF as four-pole operation (neglecting saturation) and thus better utilization of the converter dc bus voltage. Fig. 5b shows that the current in this case does not exceed the rated current of four-pole operation. In the same time the dc bus voltage capability is not exceeded, since the stator voltage required at 6340 rpm is still less than the four-pole stator voltage at 3650 rpm as illustrated in Fig 5a. This is due to that the voltage drop across the leakage inductance in two-pole operation is approximately half of that in four-pole operation at the same current level and speed. The increase in flux level for two-pole operation has negligible effect on the power factor (Fig. 5c) or input kVA (Fig. 5e). Meanwhile, due to the reduction of the ratio $\frac{i^*_{qs2}}{i^*_{ds2}}$, the slip frequency is further reduced to become about 40% of that of four-pole operation for the same output power. The 25% increase in I^*_{ds2} results in a reduction in copper losses balanced by an increase in iron losses resulting in approximately the same efficiency above 3600 rpm. Hence, it can be concluded that by increasing I^*_{ds2} by 25%, field weakening operation can be extended by electronic pole changing at 3600 rpm without exceeding the converter voltage/current rating or decreasing the output power.

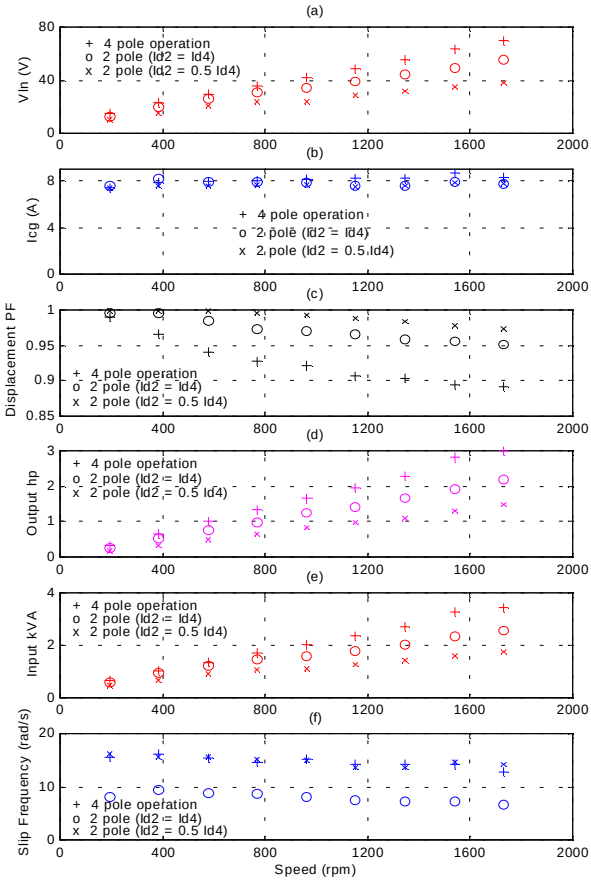

Fig. 6. Constant torque load experimental results

B. *Constant Torque Load*

The second load used to evaluate the proposed drive performance is a separately excited dc. The induction motor current level is limited to its rated value (8 A rms/coil group) and the d-axis current component (and hence rotor flux) is held constant throughout the operating range. The experimental test results for constant torque load are depicted in Fig. 6. Four-pole operation is at rated magnetizing current (3.1 A rms/coil group) which would correspond to a rated d-axis current of $i_{d4s} = \sqrt{3}\,(4.06)$ A (in case of a power invariant transformation). This leads to an almost constant torque profile (12.3 N·m) as the speed is increased till rated speed (1730 rpm) at rated output power (3 hp). In case of two-pole operation, if $i_{d2s} = i_{d4s}$ then $\frac{L_{m2}}{L_{m4}} = 1.2$ which would correspond to a rotor flux density (in the radial direction) in two pole operation of $B_{r2} = 0.75\,B_{r4}$ (from 7). The rotor core flux density would be $B_{c2} = 1.5\,B_{c4}$ resulting in core saturation.

On the other hand, if $i_{d2s} = 0.5\, i_{d4s}$ then $\frac{L_{m2}}{L_{m4}} = 1.9$, which would correspond to a rotor flux density in two-pole operation of $B_{r2} = 0.6\, B_{r4}$. In this case the rotor core flux density is $B_{c2} = 1.2\, B_{c4}$ which is not enough to saturate the core. Fig. 6a illustrates this result with the stator voltage in two-pole being approximately 75% and 60% of the four-pole stator voltage. At low speeds the stator resistance voltage drop (which is the same for all three cases) becomes preeminent resulting in an increase of the ratio between two-pole and four-pole stator voltages. The decrease in d-axis current increases the power factor as expected but the output torque (and power) is 75% and 50% of the four-pole for $i_{d2s} = i_{d4s}$ and $i_{d2s} = 0.5\, i_{d4s}$ respectively. Due to the same copper losses in all three cases but different output power, the efficiency is highest for four-pole operation and lowest for two-pole operation with $i_{d2s} = 0.5\, i_{d4s}$.

IV. Non-Linear Magnetic Analysis

The effects of main flux saturation on the machine inductances (and hence performance) are studied with the aid of finite element analysis (FEA). The nature of the magnetic flux distribution and saturation progression is investigated in both four-pole and two-pole modes.

A. Flux Distribution and Average Self Inductance

An FEA magnetostatic solution is used to model the no-load condition. Fig. 7 shows the maximum flux density as a function of magnetizing current for both four-pole and two-pole operation. At lower excitation levels, the maximum flux density is higher for two-pole operation and this trend reverses at higher excitation levels. This phenomena can be explained by the fact that saturation for four-pole operation starts in certain teeth and as the current level is increased more teeth would get saturated but saturation remains in the teeth occupying approximately the same length of the flux path (except for very deep saturation where the core would start to saturate). So the only increase in the total iron saturated area is due to the increase in the cross section area of the saturated flux path. For two-pole operation, at low current levels a very small area of the stator back iron starts to saturate and as the excitation level is increased, the saturated area starts to expand throughout the whole core. This means that in this case, there is an increase in both the cross section area and the length of the saturated flux path. Thus as the excitation level increases, the total saturated area of the magnetic circuit increases at a much higher rate for two-pole operation than for four-pole operation leading to the maximum flux density increasing at a lower rate.

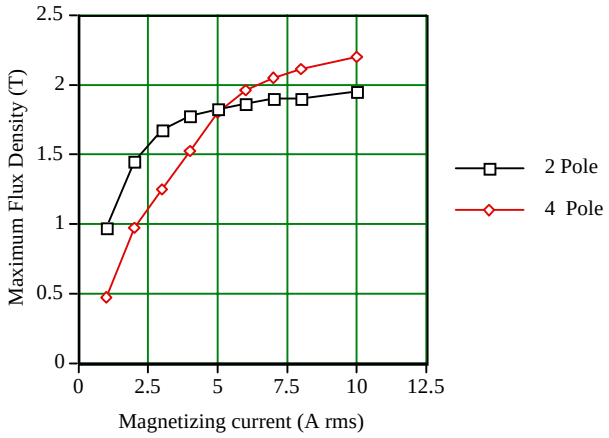

Fig. 7. Maximum flux density as a function of magnetizing current level

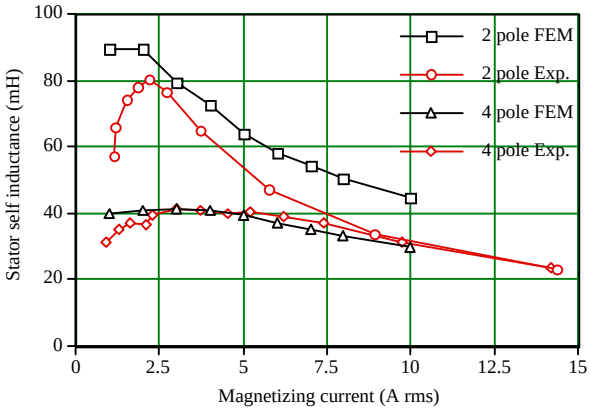

Fig.8. Average stator inductance as a function of magnetizing current from FEA and experiment

The finite element field simulator was employed to calculate the no-load inductance matrix based on the stored magnetic energy. The stator phase inductances (L_{aa}, L_{bb}, L_{cc}) obtained from the finite element results, can be used to obtain the average stator self inductance as:

$$L_{savg} = \frac{3}{2}\frac{(L_{aa} + L_{bb} + L_{cc})}{3} \qquad (9)$$

Fig. 8 shows the average stator self inductance as a function of magnetizing current for both modes of operation. The self inductance ratio starts at around 2.5 for the unsaturated case and drops to about 1.5 at high saturation. The experimental results from the no-load test show a similar trend for the self inductance but the ratio starts at around 2 for the unsaturated case and drops to about 1 at high saturation as illustrated in Fig. 8. A main difference between the finite element and experimental results is the drop of inductance value at very low voltage (current) levels for the no-load test especially for two-pole operation. This is due to the mechanical loss becoming relatively significant

at this operating point requiring an "active" current component and thus an increase in the slip.

B. Saturation Induced Inductance Variation

Another phenomena that usually accompanies saturation is the dependence of each phase inductance value on the resultant instantaneous air gap flux vector direction. Previous work incorporating teeth saturation only [14] or based on B-H saturation curves [15], [16], suggest that the $d-axis$ inductance becomes smaller than the $q-axis$ inductance (opposite to the saliency effect of salient pole synchronous machines). To investigate the dependence of this phenomena on the mode of operation, a balanced three phase sinusoidal no-load current is assumed:

$$\begin{aligned} i_a &= I_m \cos(\theta_f) \\ i_b &= I_m \cos\left(\theta_f - \frac{2\pi}{3}\right) \\ i_c &= I_m \cos\left(\theta_f + \frac{2\pi}{3}\right) \end{aligned} \qquad (10)$$

Fig. 9 shows the stator phase inductances as θ_f is varied from 0 to $\frac{\pi}{2}$ for both modes of operation at rated magnetizing current. It is clear that there is a second harmonic superimposed on each of the phase inductances. The phase inductances can be approximated from Fig. 9, as:

$$\begin{aligned} L_{aa} &= \frac{2}{3} L_{savg} - L_{sat1} \cos(2\theta_f) \\ L_{bb} &= \frac{2}{3} L_{savg} - L_{sat1} \cos\left(2\theta_f + \frac{2\pi}{3}\right) \\ L_{cc} &= \frac{2}{3} L_{savg} - L_{sat1} \cos\left(2\theta_f - \frac{2\pi}{3}\right) \end{aligned} \qquad (11)$$

where :

L_{sat1} is the magnitude of the phase inductance second harmonic

Similarly, for the stator mutual inductances:

$$\begin{aligned} L_{ab} &= -\frac{L_{ms}}{2} - L_{sat2} \cos\left(2\theta_f - \frac{2\pi}{3}\right) \\ L_{ac} &= -\frac{L_{ms}}{2} - L_{sat2} \cos\left(2\theta_f + \frac{2\pi}{3}\right) \\ L_{bc} &= -\frac{L_{ms}}{2} - L_{sat2} \cos(2\theta_f) \end{aligned} \qquad (12)$$

The dependence of L_{sat1} value on the saturation level for both operation modes can be obtained by varying the magnetizing current as shown in Fig. 10. For very low flux levels, L_{sat1} acquires a small negative value $(< 0.02\ L_{savg})$ which is within the finite element error tolerance. As the magnetizing current level increases, L_{sat1} increases with the two-pole mode case being at a higher initial rate that corresponds to the higher decay rate of L_{savg} (Fig. 8).

For a balanced three phase stator supply and winding distribution, the resulting rotating field coincides with the magnetic axis of each phase at the instant when the current in that phase is maximum. Thus at $\theta_f = 0$, the air gap flux density vector coincides with phase a magnetic axis.

Since the point where the flux in the core reaches a maximum is 90 electrical degrees from the point where the air gap flux density is a maximum, then teeth and core saturation occur spatially at a 90^o electrical apart, which would suggest that maximum phase a inductance for two-pole mode would occur at $\theta_f = 0$. On the contrary, from (11) and Fig. 10, phase a inductance is minimum at that instant, for either two-pole or four-pole operation. The portion of the magnetic circuit belonging to phase a is most saturated (regardless of saturation location) when the current in it is maximum.

The inductance matrix $[L_{ss}]$ whose elements are defined by (11) and (12), can be transformed to a rotating reference frame attached to the magnetizing current vector by [11]:

$$[L_{dqss}] = [T(\theta_f)][L_{ss}][T(\theta_f)]^{-1} =$$

$$\begin{bmatrix} L_{savg} + \frac{L_{sat1}}{2} + L_{sat2} & 0 & \frac{L_{sat1} - L_{sat2}}{\sqrt{2}} \cos(3\theta) \\ 0 & L_{savg} - \frac{L_{sat1}}{2} - L_{sat2} & \frac{L_{sat1} - L_{sat2}}{\sqrt{2}} \sin(3\theta) \\ \frac{L_{sat1} - L_{sat2}}{\sqrt{2}} \cos(3\theta) & \frac{L_{sat1} - L_{sat2}}{\sqrt{2}} \sin(3\theta) & L_{ls} \end{bmatrix} \qquad (13)$$

From (13) it is clear that the $d-axis$ inductance is smaller than the $q-axis$ inductance in either four-pole or two-pole mode with the "saturation induced saliency" effect being more evident in the two-pole mode.

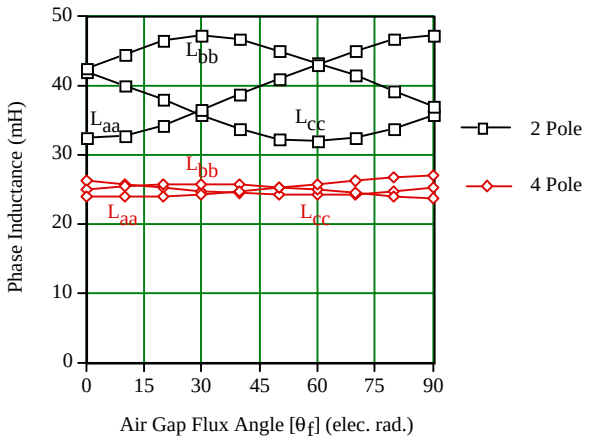

Fig. 9. Stator phase inductance as a function of the air gap flux angle at rated magnetizing current

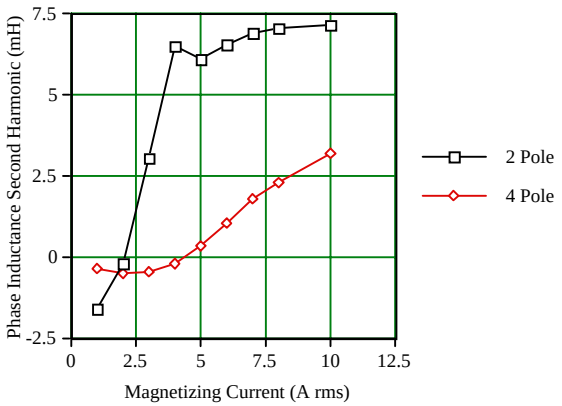

Fig. 10. Phase inductance second harmonic magnitude as a function of magnetizing current

C. *Saturation Influence on Drive Capability*

Experimental results of section III.B show that two-pole operation at rated stator and magnetizing current levels results in about 75% of the rated torque at four-pole operation. This conclusion can be verified by the finite element results. The same rated magnetizing current (6.2 A rms) leads to saturation of most of the stator back iron core in two-pole operation which reflects in a decrease in the relative ratios of the two-pole and four-pole magnetizing inductances (Fig. 8) from 2 at no-saturation to 1.5 (in FEA) or 1.2 (in experiment) at rated excitation. Consequently, the ratios of the induced air gap voltages and hence the output torque and power decrease.

The proposed pole-changing drive experimental results of section III.A can be explained with the aid of the finite element results of Fig. 7. Four-pole operation is at rated flux till 1800 rpm with the maximum flux density in the teeth being $B_{\max} = 1.94\,T$. Above rated speed, four-pole constant power operation continues till 3600 rpm with the excitation level reducing to one half the rated value resulting in the maximum tooth flux density dropping to $B_{\max} = 1.25\,T$. Switching to two-pole operation while maintaining the same magnetizing current level results in the maximum flux density occurring in the core: $B_{\max} = 1.68\,T$. Due to the poorer winding factor a 20% reduction in power capability would result. A 25% increase in magnetizing current results in retaining rated power without over saturating the core since the maximum core flux density would be $B_{\max} = 1.77\,T$.

V. Conclusions

The steady state capability characteristics of the proposed pole change drive is verified experimentally for both four-pole and two-pole operation It is proven that for a constant power load, the drive can operate at 6340 rpm in two-pole mode without exceeding either the voltage or current limits at 3600 rpm in four-pole mode. This is accomplished due to the better power factor in two-pole mode resulting in lower input kVA for the same output power. Moreover, by the proper choice of flux level to slightly saturate the core, the dip in the power capability characteristics (expected in [8]), can be avoided. A constant torque load is also employed to demonstrate the superiority of four-pole operation at lower speeds. Due to core deep saturation, a rated flux component current command results in only 75% output torque in two-pole operation.

In the latter part of the paper, the effects of main flux saturation on the machine inductances (and hence performance) are studied with the aid of finite element analysis . The nature of the magnetic flux distribution and saturation progression is investigated in both four-pole and two-pole modes. It is concluded that as the excitation level is increased, the total saturated area of the magnetic circuit increases at a much higher rate for two-pole operation than for four-pole operation while the maximum flux density increasing at a lower rate. The self inductance dependence on the excitation level is identified and compared to the experimental tests. The saturation induced inductance variation is investigated and its influence on the dq inductance matrix is quantified. In spite of saturation occurring in different portions of the magnetic circuit, the saturation induced second harmonic inductance has the same polarity in both four-pole and two-pole modes. The FEA also aided in explaining the saturation influence on the electronic pole change drive capability. Despite the change in magnetic circuit when changing from four to two-pole operation, the same power capability can be maintained due to appropriate adjustment of the flux level.

Appendix
Machine Parmeters Used IN Experiment And Simulation Studies

Per phase parameter	Four Pole Connection	Two Pole Connection
Stator resistance	0.453 Ω	0.422 Ω
Rotor resistance	0.281 Ω	0.277 Ω
Stator leakage inductance	1.31 mH	1.15 mH
Rotor leakage inductance	1.31 mH	1.15 mH
Unsat. magnetizing induct.	40 mH	79 mH

Acknowlegment

The authors wish to thank the National Science Foundation for funding of this work and the industrial sponsors of the Wisconsin Electric Machines and Power Electronics Consortium for facilities provided.

References

[1] A. Boglietti, P. Ferraris, M. Lazzari and F. Profumo, “A New Design Criteria for Spindle Induction Motors Controlled by Field Oriented Technique”, Electric Machines and Power Systems, 1993, Vol. 21, pp. 171-182.

[2] T. Kume, T. Iwakane, T. Sawa, T. Yoshida and I. Nagai, “A Wide Constant Power Range Vector-Controlled ac Motor Drive Using Winding Changeover Technique”, IEEE Trans. Industry Applications, Vol. 27, No. 5 Sept./Oct. 1991, pp. 934-939.
[3] A. Boglietti, M. lazzari, M. Pastorelli, W. Viglietti, "Induction Motor Winding Commutation with Direct Field Oriented Control for Wide Constant Power Range Operation", IEEE-IAS Annual Meeting, 1996, pp. 551-557.
[4] M. Osama and T. A. Lipo, “A New Inverter Control Scheme for Induction Motor Drives Requiring Wide Speed Range", IEEE Trans. Industry Applications, Vol. 32, No. 4, July/Aug. 1996, pp. 938-944.
[5] H. Eichhofer, V. V. Sastry and H. Weh, "Wechselrichtergespeiste Asynchronmachinen mit elektronischer Polumschaltung", ETZ-b, Bd. 28, 1976, H.5, pp. 116-118 (German).
[6] T. A. Lipo and M. Osama, "Inverter-Controlled Induction machine with an Extended Speed Range", US patent No. 5650707, July 1997.
[7] M. Mori, Y. Kido, T. Mizuno, T. Ashikaga, I. Matsuda and T. Kobayashi, "Development of an Inverter-Fed Six- Phase Pole Change Induction Motor for Electric Vehicles", International Electric Vehicle Symposium, Oct. 13-16, 1996.
[8] M. Osama and T. A. Lipo, “Modeling and Analysis of a Wide-Speed-Range Induction Motor Drive Based on Electronic Pole Changing", IEEE Trans. Industry Applications, Vol. 3, No. 5, Sept./Oct. 1997, pp. 1177-1184.
[9] D. W. Novotny and T. A. Lipo, "Vector Control and Dynamics of AC Motor Drives", London, U.K., Clarendon Press, 1996.
[10] A. M. Dudley and S. F. Henderson, “Connecting Induction Motors”, Mcgraw-Hill Book Company, Inc., 1960.
[11] P. C. Krause, O. Wasynczuk and S. D. Sudhoff, "Analysis of Electric Machinery", IEEE Press, 1995.
[12] S. Williamson and M. J. Robinson, "Calculation of Cage Induction Motor Equivalent Circuit Parameters Using Finite Elements", IEE PROC.-B, Vol. 138, No. 5, Sept. 1991.
[13] S. Williamson, R. E. Knight and I. W. White, "Implementation of Finite-Element Analysis in a Cage Induction Motor", 7th International Conference on Electric Machines and Drives, 1995, pp. 57-61.
[14] J. C. Moreira, "A Study of Saturation Harmonics with Applications in Induction Motor Drives", Ph.D. Thesis, University of Wisconsin-Madison, 1990.
[15] J. E. Brown, K. P. Kovacs and P. Vas, "A Method of Including the Effects of Main Flux Path Saturation in the Generalized Equations of ac Machines", IEEE Trans. Power Apparatus and Systems, Vol. PAS-102, No. 1, Jan. 1983.
[16] M. Osama, K. Sakkoury and T. A. Lipo, "Transient Behavior Comparison of Saturated Induction Machine Models", IMACS-TC1 '93 Conference Proceedings, pp. 577-580.
[17] T. A. Lipo, “Introduction to AC Machine Design”, WISPERC, 1996.
[18] M. Osama, "A Wide-Speed-Range Induction Motor Drive Based on Electronic Pole Changing", Ph.D. Thesis, University of Wisconsin-Madison, 1997.